

MEASURING SMALL FATIGUE CRACK GROWTH WITH THE AID OF MARKER BANDS IN RECRYSTALLIZATION ANNEALED Ti6Al4V

Ingrid Kongshavn¹, Simon Barter² and Larissa Sorensen³

¹ RUAG AG, Ingrid.Kongshavn@ruag.ch

² RMIT University

³ RUAG AG

Abstract: Titanium alloys are used in fighter aircraft in highly stressed locations to improve fatigue resistance in fracture critical structural parts. Examples include the F-35, with a main bulkhead of titanium Ti6Al4V beta annealed (BA) and the main bulkheads of the Swiss-specific F/A-18C/D that are recrystallization annealed (RA) Ti6Al4V. A benefit of the RA over the BA Ti6Al4V microstructure is that fatigue cracks can remain very small for a long portion of a component's life due to initially slow crack growth. Small cracks, those generally less than 1mm deep, are difficult to find and track in coupon tests and in complex structures such as in full-scale fatigue tests. Since such cracks spend a considerable period of their life at small sizes, information about their growth while they are small is often of great use. This can be achieved by post-test quantitative fractography (QF), which allows crack growth measurements over the full range of crack depths. To aid QF, distinctive loads may be added in the form of ‘marker bands’; specially designed loading cycle sets that introduce recognisable fracture surface marks. Unfortunately, the interpretation of QF markers on RA Ti6Al4V fracture surfaces can be especially challenging at smaller crack sizes due to the small multi-phase microstructure. To improve the likelihood of being able to ‘read’ such fracture surfaces by QF, this paper discusses a methodology used to develop markers for this material. The effectiveness of the method is presented with an example of one of many crack growth curves produced. Observations about the nature of the fatigue cracking during the first 0.25mm of growth (‘engineering crack initiation life’) are also described, including comparisons to crack growth in BA Ti6Al4V.

INTRODUCTION

Synonymous with the changing demands of a world in transition, technology supporting aircraft structural integrity must continually evolve for aircraft to perform better, fly cheaper, reduce risks and be available longer. In many cases, the aircraft themselves are in a technology transition, containing a mix of legacy materials and now, new additively manufactured parts. An example is the implementation of forged

recrystallization annealed (RA) Ti6Al4V in the Swiss F/A-18 bulkheads, versus the more recent choices of heat treatment for this material, such as the use of beta annealed (BA) ELI Ti6Al4V in the F-35. To evaluate the fatigue life of such parts, modern methods focus on a holistic lifing approach that includes the determination of crack growth rates from very small crack sizes until failure. The small crack growth regime is typically defined as cracks smaller than about 1mm [1]. One older [2], yet evolving method for measuring crack propagation is the use of quantitative fractography (QF). This method has successfully and extensively been applied to aircraft structural materials such as aluminium and steel alloys [3]. However, studies of its use at small crack sizes, for complex dual phase microstructures such as those found in titanium alloy structural components, are less common.

Successful QF measurement of fatigue crack propagation on a fracture surface requires good visibility of marks that can be correlated to the loading. The visibility and identification of these markings is highly dependent on the interaction between intrinsic material properties such as the microstructure and the available deformation systems (slip systems and/or twinning), on the phases present, and on the extrinsic parameters such as the loading sequence, load level, local geometry, and stress distribution. While some marking of fracture surfaces may occur naturally from the loads in a variable amplitude (VA) spectrum, the addition of artificial markers in the form of specially designed additional loading cycles will ensure that the crack propagation can be reliably measured.

The purpose of the research presented in this paper was to produce crack growth information using marker loads for a life assessment of the Swiss F/A-18 RA Ti6Al4V wing carry-through bulkheads. Given the structural significance of the centre barrels, their design relied on this alloy and the RA heat treatment in order to optimize the crack initiation resistance properties of the bulkheads. The bulkheads must now be re-evaluated as the consequence of a life extension requirement for the Swiss F/A-18 fleet; a 20% increase in the Swiss service life from 5000-6000 flight hours. A full-scale test of the Swiss centre barrel (including the three titanium bulkheads) is currently being performed in a collaborative test program between the Swiss Federal Council (armasuisse) and the Australian government (DSTG), called the Swiss Titanium Research Experiments on the Classic Hornet (STRETCH). To support this test and the general life extension, supporting coupon tests were carried out.

The process used to develop ‘marker bands’ (MBs or ‘markers’) to aid QF measurements of fatigue crack growth in the die forged RA Ti6Al4V material of the Swiss bulkheads is presented. The aim was to gather crack growth data from as close to the origins as possible, and particularly within the first 0.25 mm of growth, to support the establishment of the ‘engineering crack initiation life’ (CI). Images of the block repeats and the markers are presented at various crack depths, along with observations about the nature of cracking prior to CI crack depths. The gathering of crack growth data for small cracks in this material is fairly unique.

QUANTITATIVE FRACTOGRAPHY OF FATIGUE CRACKS

Fractography is a well-known method [4][5] for studying the nature of material failure through the examination of fractures. Quantitative fractography [2] attempts to quantify fracture features and correlate them to the material's microstructure, environment and the loading that caused the fracture. In the case of fatigue cracking, it has been used successfully to assess the nucleation and growth of cracks post failure, by matching fracture surface features to the loading applied [3]. QF is very useful for measuring growth during testing while cracks are small, when they are often difficult to detect and measure with real time

surface length techniques. Moreover, QF comes into its own in the assessment of full-scale fatigue test cracks and service failures, where the application of controlled crack growth measurement methods during testing is often not possible. Understanding crack growth during its total life is important to manage fleet structural integrity, to determine CI life, to define fleet inspection intervals, and to develop effective repairs [6][7][8][9][10][11]. It also gives confidence in crack prediction tools by providing corroboration with real crack growth measurements [12][13][14].

The features that allow the post-test measurement of crack growth are usually the result of the nature of the loading, the rate of the cracking and the environment [2]. For constant amplitude (CA) loading cycles, rates are not usually measurable until individual striations are observed. At best, striations can be counted, via high resolution Field Emission Scanning Electron Microscopy – FEG-SEM, for growth rates from about 2×10^{-8} m/cycle. However, with CA loading the usefulness of single cycle counting tends to be for rates closer to 2×10^{-7} m/cycle due to large variations in local growth rates, difficulties in measuring such small features and their intermittent appearance on a fracture surface [11].

When loads are varied, for example by applying either blocks of VA or CA loads, high loads, high delta loads, or underloads etc., this can produce marks on the fracture surface delineating bands of crack growth. These bands can be measured at a growth of about 2×10^{-8} m/band. These bands are more reliably counted at rates beyond 5×10^{-8} m/band. This is better than can be achieved for single cycle counting, since the measurements are of an average growth rate per band [12]. Indeed, under optimal conditions, bands of CA loads within a VA spectrum can produce clearly recognisable markings, thereby allowing cracks to be measured down to a few microns from a nucleating feature [13], where single striations would not be visible. This technique has been effective for the measurement of very small crack growth increments in high strength aluminium alloys [12]. Unfortunately, in the case of poorly marking materials such as RA Ti6Al4V, or poorly marking spectra, careful additions of marking loads are required to allow at least some of the very small growth rates to be measured.

MARKER LOADS FOR FATIGUE CRACK MEASUREMENT IN RA Ti6Al4V

Ti6Al4V is a dual phase material consisting of a hexagonal close packed (HCP) alpha (α) phase, and a body centred cubic (BCC) beta (β) phase. At room temperature, the α phase is the stable form of titanium and in Ti6Al4V it is generally the dominant phase. Through the presence of the β stabilizing vanadium, the normally high temperature β form of titanium is also stable at room temperature, tending to remain at the α grain boundaries as ribs or islands. Due to their different crystal arrangements, fatigue cracks tend to take different paths in these two phases while they are small. The result is rough fracture surfaces, and this roughness is further exacerbated at low driving forces due to the limited slip systems in the α . Under these conditions, cracks tend to follow the close packed basal plane of the HCP structure [20]. In fine grained alpha, where the crystals are misoriented to one another, this produces fatigue fracture surfaces that are cluttered with path change artefacts. For small α grain sizes of about $10 \mu\text{m}$, as in RA Ti6Al4V (shown in Figure 1A), the short distances travelled by a crack before hitting an α grain boundary or a β rib produce very short planes of flattish growth. This results in a rough topography with many path changes, increasing the challenge of measuring a consistent crack growth curve or determining a representative crack growth rate. For those microstructures that have large packets of aligned α plates or laths within prior β grains, as in beta annealed (BA) Ti6Al4V, the tendency of the cracking to be aligned with the basal plane of the α plates introduces large scale (due to the large packets) flat regions in which growth planes are of the order of the packet size. Roughness is thus on the order of the prior β grain size. An example BA Ti6Al4V

microstructure is shown in Figure 1B, where packet diameters of about 1mm containing aligned α plates can be seen. Compared to RA, this results in longer distances between the gross path changes where marking load features can be more easily seen and measured. Marking is therefore vastly easier in BA material, although the large-scale roughness still introduces challenging fractures upon which to carry out QF. Consequently, compared to high strength aircraft aluminium alloys and BA material, where markers can be reasonably easily introduced, as shown for example in Figure 2A and Figure 4, the deliberate marking of RA Ti6Al4V material is difficult for small crack sizes; sub 1mm. Furthermore, there is little literature available to guide in the development of reliably visible MBs for small crack growth measurements in RA material.

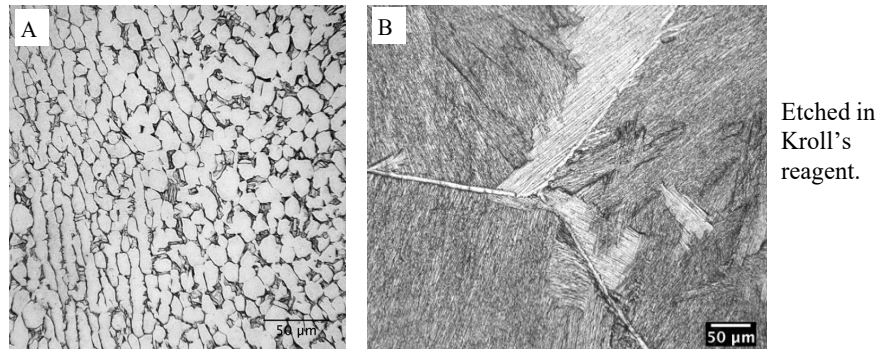


Figure 1 A: RA Ti6Al4V microstructure and B: BA microstructure. Light areas are α phase and dark areas β phase. Note the equiaxed α in the RA and aligned α laths in large ‘packets’ in the BA material.

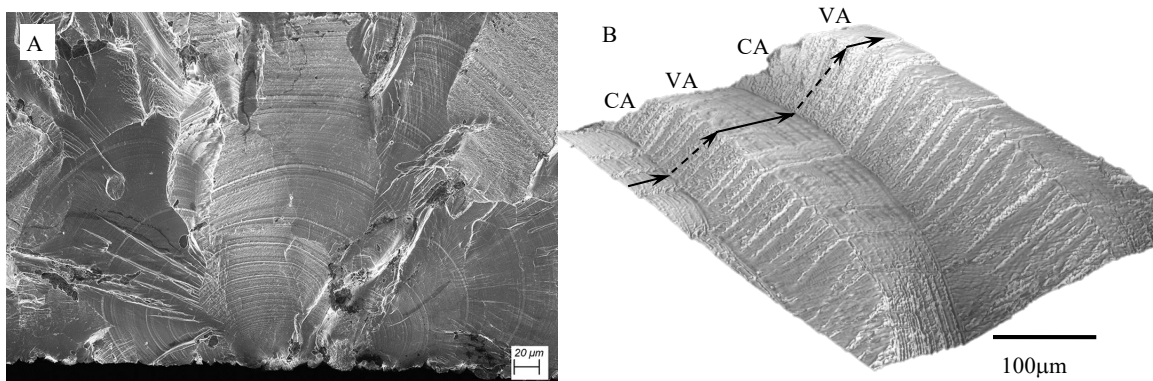


Figure 2 A: Origin region of an aluminium alloy crack with MBs added. The high R (stress ratio = $\sigma_{\min}/\sigma_{\max}$) CA bands in the marker band are light bands, visible at very small crack sizes. B: high R CA blocks can be seen to change the crack path and topography from those of the low R average VA loading.

The following methods, based on loads manipulation, have been used with some success to mark various metal alloy fatigue cracks [2][6][14][15]:

1. adding loads higher than the peak load in the spectrum. These can be enhanced by the addition of underloads, either applied prior to a high load to increase the delta, or after the high load to reduce the overall effect of potential retardation;
2. adding CA loading blocks that may have a constant max stress and a varying mean stress, or a varying max and mean stress;
3. using combinations of the above to create 'bar-coded' MBs [14][15] [16];

4. reordering the max and/or min peaks in a spectrum to create the benefits of over/underloads while minimizing changes in the effects of retardation;
5. reordering blocks of loads in a spectrum to create a distinctive pattern for the VA loading.

Of these methods, CA block patterns, with constant peak load values less than the peak in the spectrum, have been found to be very useful and are the starting point for this study. Work on marker loads in aluminium and subsequently on BA Ti6Al4V [14][15] has shown that CA blocks added to a VA spectrum produce path and topography/texture changes. For example, Figure 2B shows a 3d rendition of high R CA bands with intermittent VA bands. This has resulted in growth on notably different planes between the two types of bands. The same effect can be produced by changing from high R CA to low R CA loading in lieu of the VA loading shown.

TESTING

The full-scale STRETCH test campaign required the development of marker bands for assessing fatigue growth in the article post-test. A coupon study was performed to establish the best marker bands that would not only work in the full-scale test, but would also allow measurement of the effects of spectrum truncation on the damage rates, through the testing of single side edge notched tension (SENT) high K_t coupons as shown in Figure 3 ($K_{t, \text{gross}} = 3.4$ from [17]). These were cut from a 101.6 mm thick, AMS 4928 RA Ti6Al4V forged plate. The microstructure consisted of fine-grained (10-20 μm) equiaxed alpha with remanent beta phase 'ribs' and islands, as shown in Figure 1A. Vickers hardness (10kg) tests gave an average of 356 HV₁₀ (four tests). To help mimic crack nucleation from the production surface finish used in the aircraft, and to reduce fatigue life scatter, the coupons were etched in a 50% nitric and 1% hydrofluoric acid bath at room temperature for 5 minutes.

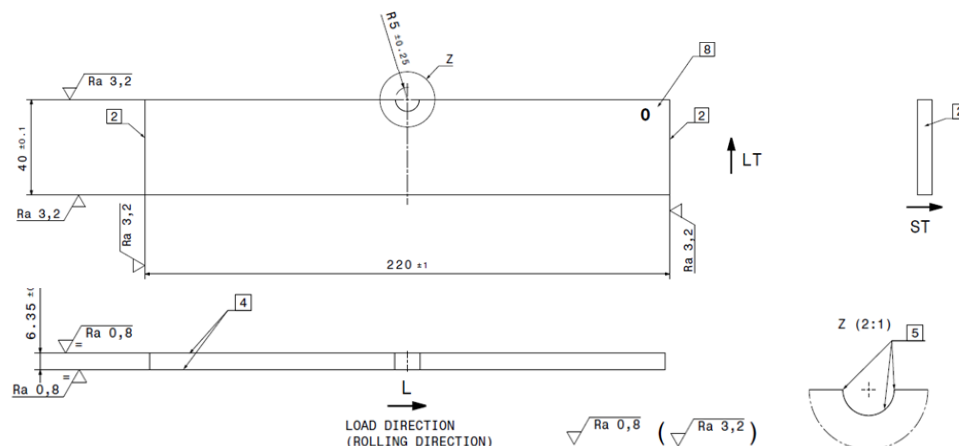


Figure 3 SENT coupon with $K_{t, \text{gross}} = 3.4$.

The VA spectrum applied to the coupons was generated from the original Swiss usage spectrum (wing root bending moment) containing over 1.3 million turning points (TP). The spectrum was reduced to 438,000 cycles for the 1% rise/fall filtered 'untruncated' spectrum and 32,000 cycles for a 9% rise/fall filtered truncated spectrum, which was to be applied to the full-scale test. Tests were carried out at two load levels roughly corresponding to one and three times the design CI life. The tests were performed by both RUAG AG and RMIT, using uniaxial servo-hydraulic test machines under load control. Table 1 shows the test matrix.

Table 1 Coupon test matrix.

Test Centre	Test type	WRBM Spectrum	TP's per Block	Peak elastic notch stress $K_t\sigma$ (MPa)	Test Frequency (Hz)	# Coupons per Load Level
RMIT	MB development / test machine tracking assessment	truncated and untruncated	~32 000-438 000	932-1278 MPa	10 - 20	12
RUAG	main tests	truncated	~32 000	1'158 / 965	11	5/5
RMIT	main tests	untruncated	~438 000	1'158 / 965	10 - 20	5/5

MARKER BAND DEVELOPMENT

In addition to the challenges of developing reliably visible markers, the following requirements were important both for coupon testing and for the full-scale centre barrel test:

- Markers should be visible in all regions of crack growth, down to very small crack sizes (0.01mm).
- Markers should be identifiable with an optical microscope, or at small crack depths with the SEM.
- Marker load damage should be less than 10% of the damage produced by the VA spectrum.

For the VA test spectrum, studies in a parallel program on 7050-T7451 aluminium alloy showed that alternating CA blocks with different R's (method 2 from the above) and a bar-code type marker (method 3) created distinct patterns, as shown in Figure 4A. This was consistent with previous studies such as [14][15]. Having two distinct bar-coded MBs had also worked in BA Ti6Al4V (an example bar-code band is included in Figure 4B) [15]. However, previous tests with RA Ti6Al4V found that the more complicated the bands became (such as the MB1 coded band shown in Figure 4), the more they tended to blend into the VA spectrum growth, defeating the advantage of the coding [15]. As noted previously, the comparatively large (effective) grain size of the BA Ti6Al4V allowed such markings to be successful, while the fine-grained RA Ti6Al4V obscured the MBs. Thus, simple MBs were more likely to be easy to find on a RA fatigue fracture surface.

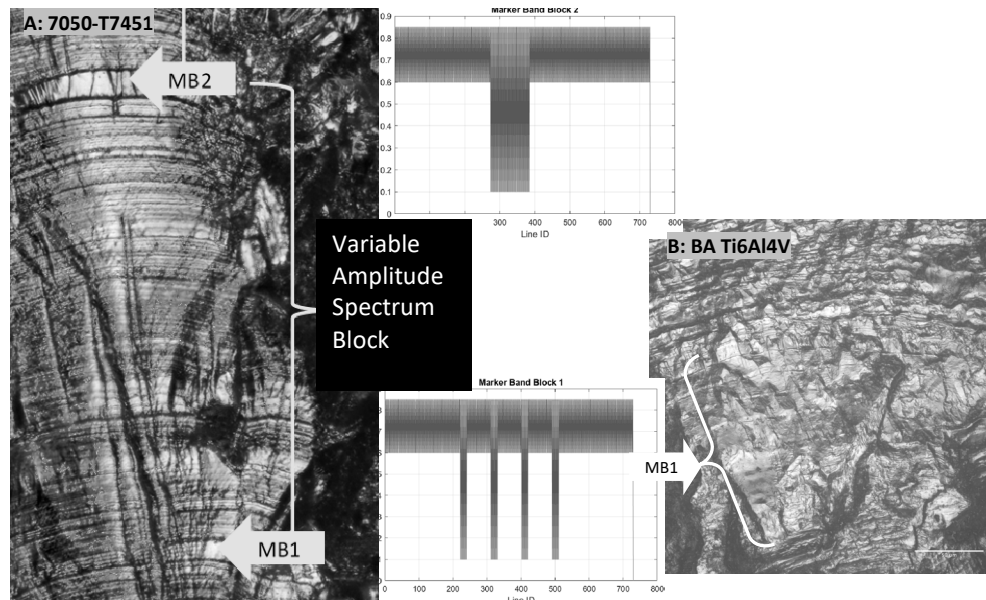


Figure 4 Optical views - A: Two CA block bar-coded MBs on AA7050-T7451, with B: MB1 also shown on a BA Ti6Al4V surface. MB1 was a more complex bar-coded MB compared to MB2.

While simplicity in the markers was important for visibility in the RA material, there were still many fracture features that were produced by the VA spectrum that tended to look similar to the tested MBs. To overcome this and to make the markers more unique, a hybrid solution of constant amplitude blocks and repositioned peak loads (methods 2 and 4) was used to develop more visible MBs without using overly large CA loading blocks. The basic marker band consisted of a low R CA load block sandwiched between two equal high R CA load blocks (high R/low R/high R). Each block had a constant peak of 90% of the maximum VA load. This load level was higher than that required for marking in aluminium testing. Keeping the peak load limited to 90% of the peak VA loads still avoided retardation issues, since this VA spectrum had a significant number of load lines above 90%. Having a large ΔK in the low R marker blocks produced visible striations relatively early in the crack growth. The numbers of low R cycles per block were kept to a minimum to avoid inducing excessive damage. The intent of the high R blocks was to break up the crack front (increase roughness) and introduce path deflection after the preceding VA block and after the low R block. The desired effect was a marker that had a ‘tram track’ appearance.

To meet the visibility requirement at smaller crack sizes while restricting the amount of growth produced by the MBs to 10% of the total growth, existing spectrum peak loads were leveraged (method 4). This improvement took a peak load from the spectrum and placed it at the end of the low R loads. The highest load was also moved to a position just after the second high R band, borrowing on the high load and underload marking methods while avoiding the disadvantage of adding excessive overloads or underloads to the spectrum. The intention was to create a clear feature that would distinguish the end of the MB. The initial marker bands developed using this combined technique are set out in Table 2.

Table 2 Initial variations of high R/low R/high R MB combinations.

Loading description*	Number of cycles in MB			
	MB1 v1	MB2 v1	MB3 v1	MB1 v2
Half cycle start at 0	1	-	-	1
High R loads 0.7-0.9	1000	999.5	1000	499.5
Low R loads 0.1-0.9	10	20	15	30
Spectrum cycle 0.022027-0.99141	1	1	1	1
High R loads 0.7-0.9	996.5	1000	1000	500
Spectrum cycle – 0.26259 to 1	1	1	1	1
Half cycle end at 0	1	1	-	1

*Normalised by the peak positive load, where the peak load would equal 1

A first version of the trial spectrum with three VA blocks and three MBs is shown in Figure 5. In addition, Figure 5 shows an optical view of the fracture surface of this first coupon where the MBs are indicated with arrows. As can be seen, the surface is very rough and the bands, although visible, are hard to see, which is typical of this material close to the origin. The roughness about the origin was usually significant and tended to lead to a lot of fracture rubbing that obscured large areas of the origin region and made it difficult to see MBs over the first few hundred microns of growth. This contrasts with the aluminium example shown in Figure 4, since aluminium alloys loaded with wing root bending moment VA spectra tend to have large relatively flat planes of growth near the origin, which facilitate recognition of markers and spectrum repeats.

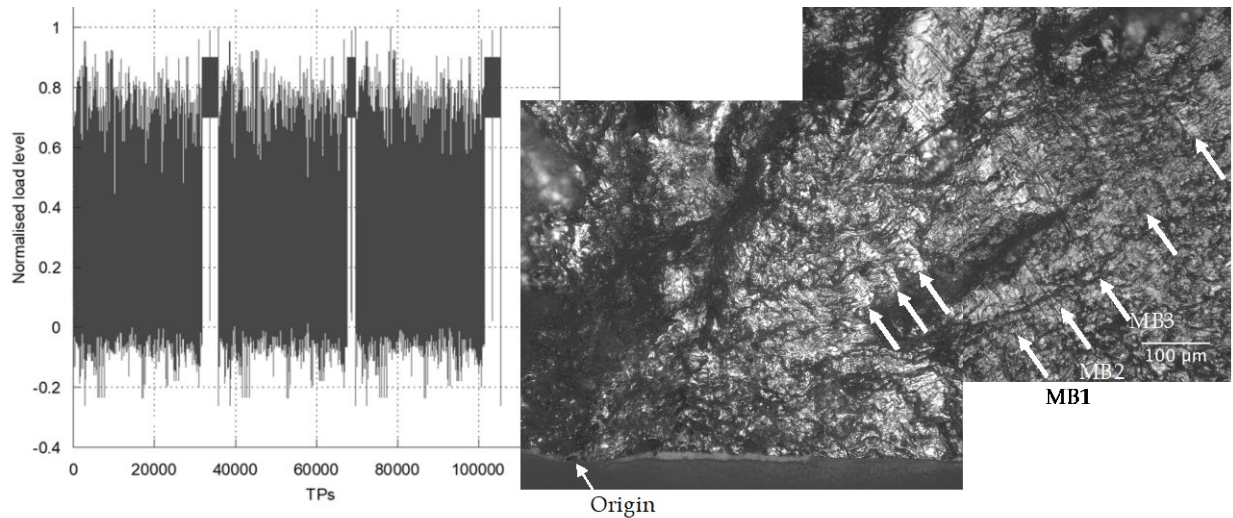


Figure 5 Loading spectrum with three combinations of high R/low R/high R MB's, and an optical view of a fracture surface showing 'tram-track' like marks that are the MBs.

The crack surface produced with the Table 2 MBs, showed that the peak load produced a clear mark in the form of a ridge at the end of the low R band. This correlated to similar observations in AA7050-T7541 [17] and in AA2024-T3 [19]. The highest peak/valley cycle that was placed at the end of the second high R band did not improve the visibility of the end of the MBs as intended, so this load pair was moved to the position just after the other high peak load, adding to the effectiveness of the low R block. This modification was tested with various combinations of numbers of loads in the CA parts of the marker, both for visibility and for the extent of damage created. This resulted in the choice of MB1 and MB2 as shown in Table 3.

Table 3 Final version of the marking scheme, consisting of two MB's. Each MB is applied alternately at the end of one VA spectrum.

	MB1	MB2
High R loads 0.7-0.9	1500	1500
Low R loads 0.05 -0.9	20	15
Spectrum cycle 0.022027-0.99141	1	1
Spectrum cycle - 0.26259 to 1	1	1
High R loads 0.7-0.9	1500	1500

To improve measurement reliability, two distinct marker band patterns were desired. These should be uniquely identifiable in at least some portions of the fatigue fractures to help in tracking growth. An alternating MB pattern added confidence by ensuring that one MB was not missed in the measurement sequence. The alternating MB was created by varying the number of low R cycles that produced countable striations. The target was to have a MB that could be identified as either MB1 or MB2 at about 0.5 mm from the origin, where it could be clearly identified using the optical microscope (up to about 1000x). The number of low R loads in MB2 was reduced compared to MB1 to minimize damage, and is shown in Table 3. A schematic of the final MB1 placed after the VA target spectrum, together with views of an RA fracture surface produced by the VA and this MB, is shown in Figure 6. The final marker provided a good 'tram-track' like appearance, which was visible in the optical microscope generally at depths above 100µm (Figure 7) and in the FEG-SEM close to the origin. The amount of growth produced by these MBs did not exceed the 10% growth limit requirement.

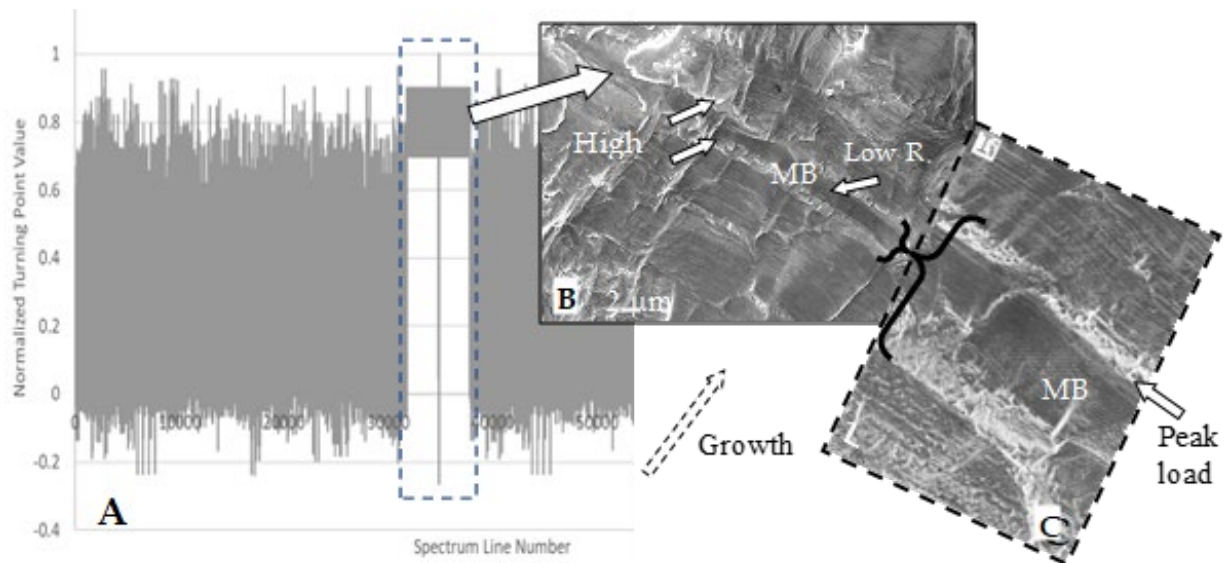


Figure 6 A: VA block with MB1. B: View of MB1 at about 1 mm from the origin. The first small white arrow indicates the first high R band, the second small arrow indicates the low R band and the third the second high R band. (Untruncated spectrum, high load level.) C: close up of the MB.

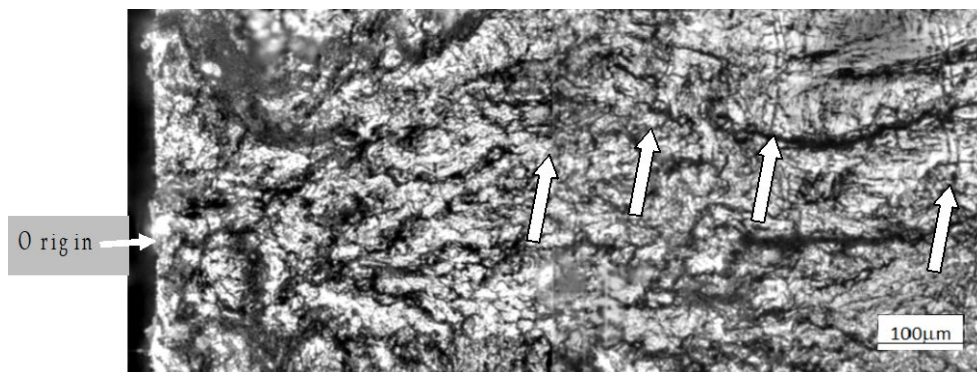


Figure 7 Optical view of MBs on the fracture surface of a truncated spectrum, high load level test.

From a macro perspective, the fracture surfaces produced in these tests were relatively easy to measure from about 1mm to the end of the crack. An example of the appearance of the markers on one of the fractures is shown in Figure 8, where several of the MBs are indicated.

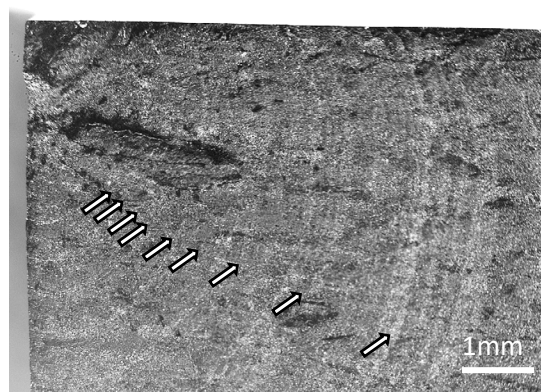


Figure 8 Optical view of an origin. Some MB's (arrows) are indicated. Low load level, untruncated.

DETAILED FRACTURE SURFACE OBSERVATIONS AND DISCUSSION

As is typical of titanium Ti6Al4V, the crack origin is often difficult to identify. This material is typically very 'clean' so that inclusions are not an initiator. The deoxidizing treatment performed prior to testing did not pit the material to any great extent, in contrast to aluminium alloys treated with the same chemicals. Nucleation appeared to occur at the surface within single α grains and to initially grow on or very close to the HCP basal plane, as has been reported for RA and BA materials [21]. This plane was usually inclined at high angles to the loading axis: ~ 45 degrees or more, thus being close to maximum shear planes. Typically, the crack appeared to grow relatively quickly within the first α grain due to its apparently favourable initial orientation. Growth then slowed as it crossed into the surrounding grains, where it was forced to re-orient its growth plane to match the crystal orientation of the next α grain. This produced a faceted appearance (Figure 9).

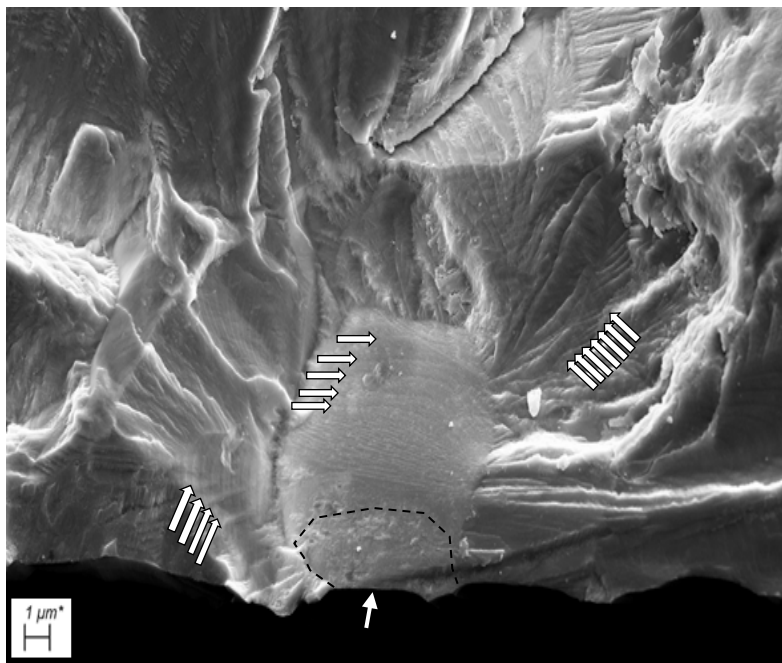


Figure 9 SEM image of a faceted origin in a low load, truncated spectrum coupon. The nucleation location at a 1-2 μ m deep etch pit is indicated. The other arrows indicate repeats of the loading spectrum.

These facets, rather than being flat and featureless, showed evidence of progression marks that appeared to be the result of the repeated VA blocks of loading, enhanced by the MBs. In several cases these could be seen clearly on the first grain, as in Figure 9, where the nucleation region is indicated. When these block repeats were measured, they were consistent with the numbers of blocks applied and the rest of the measured crack growth. The presence of the progression marks, which are the result of very local crack path changes, indicates that the growth on these facets is by Mode 1 tensile crack opening and not Mode 2 shear, or cleavage, as has been suggested [23][24][25].

As described previously, at each grain boundary the crack usually changed direction dramatically. In the region around the origin grain, the crack grew in any favourable direction on planes close to a shear plane. This could even be backwards towards the surface as can be seen in Figure 10B. The roughness often produced a good deal of rubbing that also led to fracture damage and the generation of fretting product. These features can also be seen in Figure 10A.

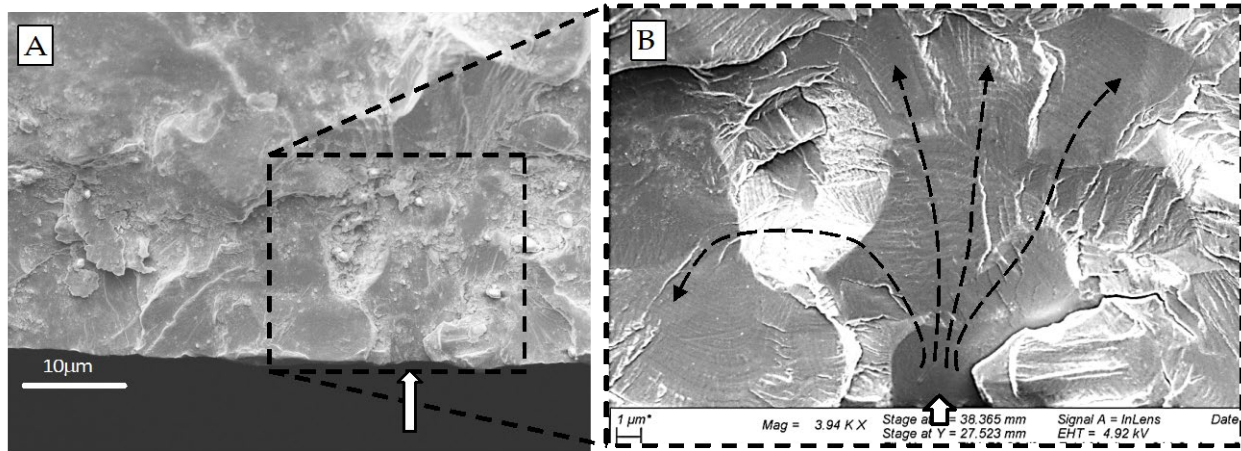


Figure 10 A: Untruncated spectrum, low load level coupon. Debris and rubbing are visible. B: Initiation site shows crack growing in different grains, on different planes, and even having to return in a backwards direction to crack through an adjacent grain.

Figure 11A shows a general view of the faceting about the origin region for a low load coupon. These faceted surfaces were often angled at 45° to the loading surface and tended to extend into the material as seen in Figure 11A. Since the crack paths followed steep angles away from the origin, this typically led to average growth planes forming on separate levels on either side (Figure 11B). This bifurcated, quasi-independent growth also added to the surface roughness and crack retardation until the separate growth planes merged to form a single crack plane.

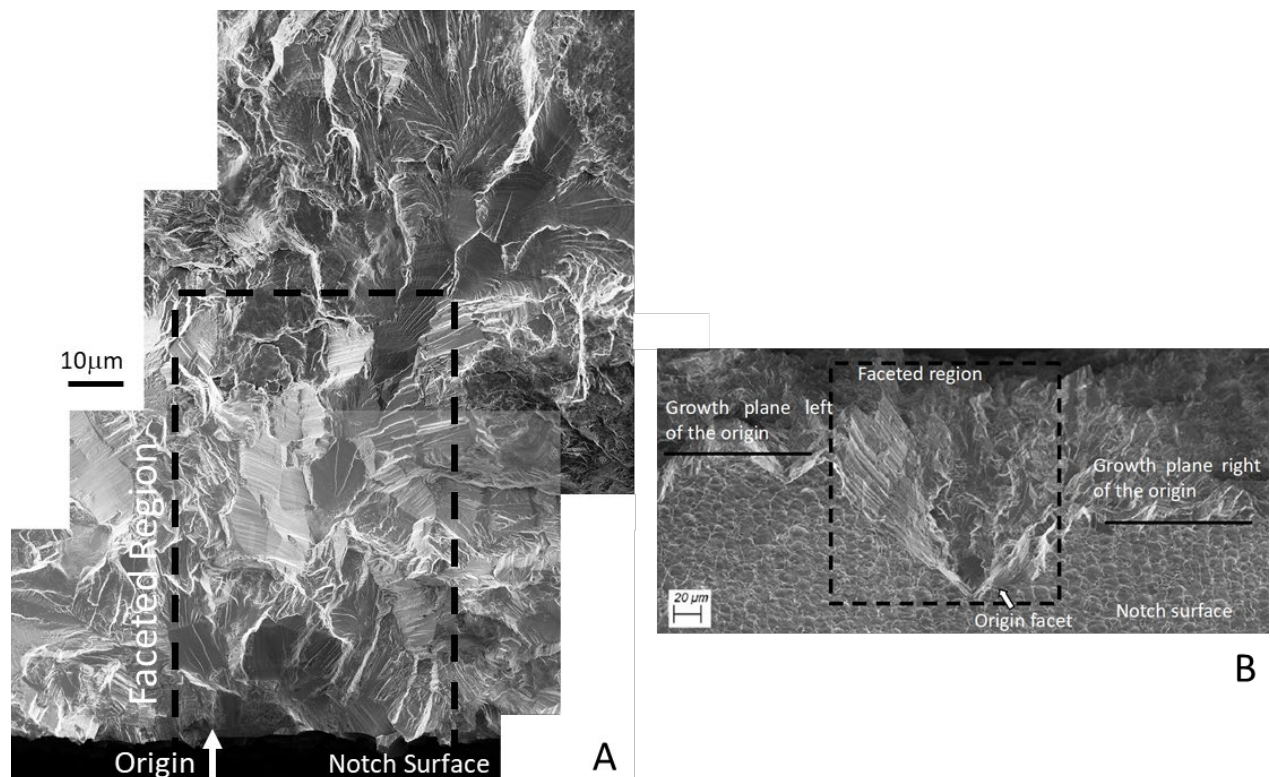


Figure 11 A: Montage of an origin region for one of the cracks. The dashed box contains the faceted region. B: View from the surface of the notch of one of the origin regions.

The roughness and steep angles of the facets seen in Figure 11 have a strong influence on the average growth rate. The rougher the surface, the slower the average growth rate will be, even if the local growth rate on a single facet is relatively fast. This is a result of a reduction in the effective ΔK at the crack tip due to crack face contact induced by misoriented facets (small scale roughness). Having steeply angled facets also reduces the effective ΔK as they are subject to a locally reduced Mode I component of the applied load, since the crack path is forced to follow the basal planes in the direction of maximum shear. While these issues may be implicit to some extent in the standard empirical da/dN data that is generated from through-section cracks in thick section coupons, this data is probably not very representative of the true propagation of these natural cracks at small sizes.

A higher magnification of the origin region shown in Figure 11A is presented in Figure 12. Several areas of repeating patterns can be seen on the facets, particularly in the expanded views, where the rates of crack growth vary considerably. In some cases, the repeats are very fine and close together (thick white arrow in 'C'), yet almost adjacent to this they are distinctly farther apart (thick black arrow in 'C'). Only a short distance further into the crack ('B'), block repeats can be seen in more detail and are growing considerably faster, with block repeats marked with thin black arrows. Consequently, the crack growth rate changes when measurements are taken across these regions, producing some rate deviation during the early part of the curve. The growth after the faceted region was less microstructurally sensitive and therefore more consistent, with a more ductile appearance. The QF curve for this fracture is presented later in Figure 13.

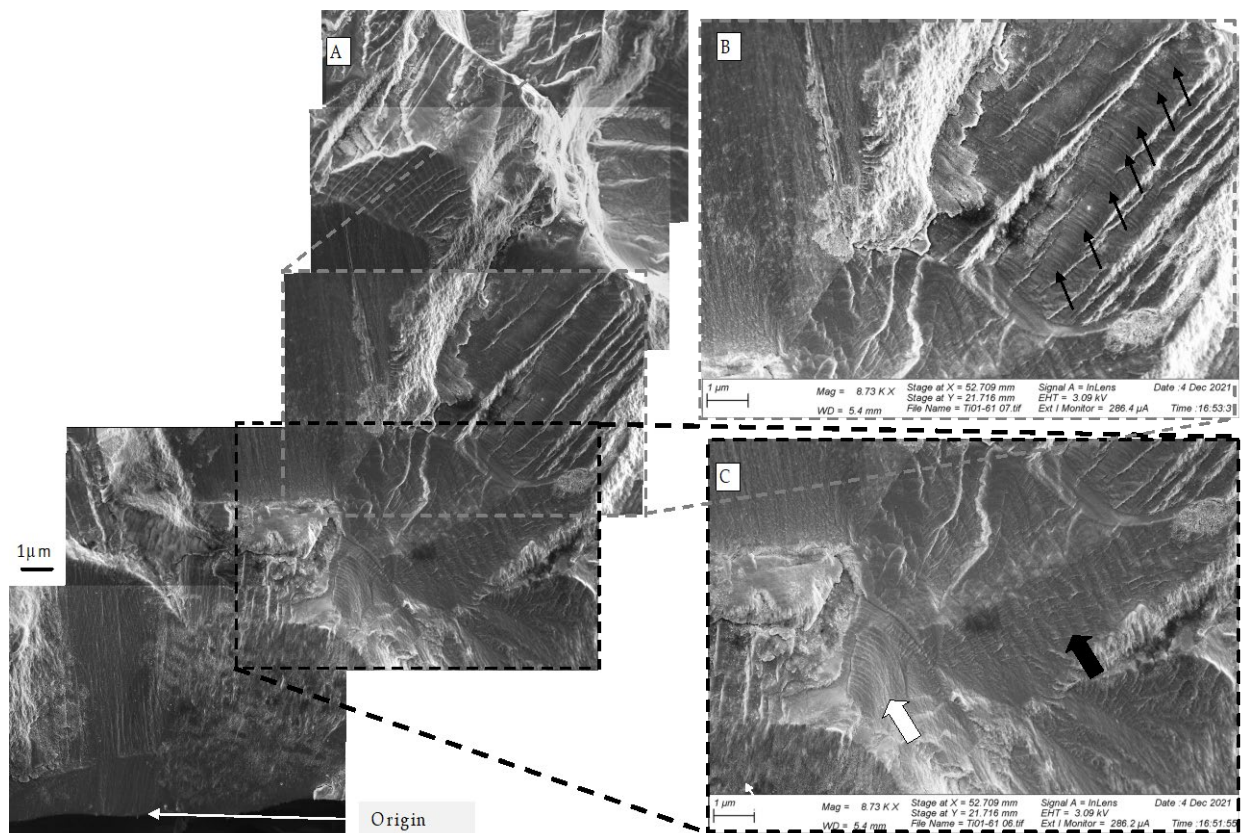


Figure 12 Origin region of a low load, untruncated spectrum coupon, up to about 35 μm depth. The inserts are expanded views showing blocks of loading that repeat at different rates.

CRACK GROWTH MEASUREMENTS

Crack growth beyond 0.1-0.2 mm could be reliably measured with the optical microscope. This corresponded approximately to the depth at which faceting was reduced and a single growth plane formed. Closer to the origin, a FEG-SEM was used for growth measurements as shown in Figure 11 and Figure 12. Regardless of the measurement method, damage due to the roughness often obscured some regions at small crack sizes. Early crack growth rates were highly dependent on individual grain orientations and local crack paths, as has been discussed. Although these growth rates varied from facet to facet, causing the curves to ‘wobble about’, it was possible to generate surprisingly complete curves for several cracks.

One example QF curve is shown in Figure 13, with exponential curve fits applied to each group of measured data points. The curve fits were used to help set the positions of the ‘orphaned’ groups of measured data to build the complete crack growth curve. There is always some uncertainty in positioning orphaned data when there is no known pegging marker available to fix a point with absolute certainty. Since there is an expectation that the growth curve will be reasonably smooth once it has extended beyond the faceted region, using exponential curve fits helps to piece a curve together despite incomplete data sets. In the case of the example shown, and for many of the crack growth curves produced, the early growth region was used to extrapolate the effective size of the nucleating equivalent crack size (EPS), which in this case was 1.4 μm . An engineering CI depth of 250 μm occurred at about 188 blocks in the third period of growth. Beyond the third period of growth, the rate increases significantly as the crack has moved out of the faceted growth region and the crack path is less tortuous. At these large crack depths, the high driving forces and plastic zone cover many grains, thereby lowering the fatigue resistance compared to the faceted region. In comparison, BA Ti6Al4V with its large packet sizes, has relatively poor resistance to small crack growth due to fewer effective grain boundary crossings. Long cracks however show good crack growth resistance.

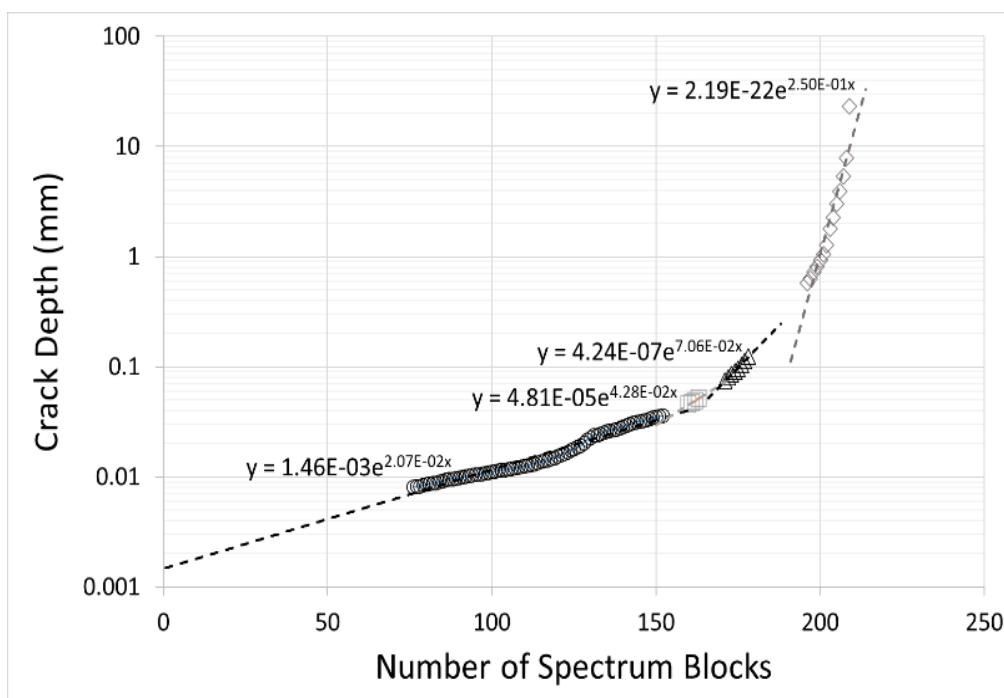


Figure 13 Plot of the measured crack depth versus block repeats, where exponential curve fits have been applied to each group of measured data. The early growth part was used to estimate the EPS, and the third period of growth was used to estimate the CI life.

CONCLUSIONS

While the microstructure of RA Ti6Al4V is advantageous for fatigue resistance, it presents additional challenges for the QF analyst, especially at small crack sizes. In this paper it has been shown that the traditional techniques used for marking aluminium and BA Ti6Al4V can successfully be applied to RA Ti6Al4V, with certain adaptations. The angled faceting and surface roughness in RA Ti6Al4V reduce the probability of grains being oriented such that the marker loads are clearly visible. It is therefore important to have a marker that is unambiguous, and will clearly stand out when a grain is fortunately oriented. This can be achieved by creating a simple but unique pattern of High/Low/High R CA blocks combined with a reordering of the naturally occurring spectrum peak loads to improve visibility.

The use of marker bands to understand crack growth mechanisms in RA Ti6Al4V is particularly useful near the crack origin and at small crack depths. Such markers help to visualize the growth within the single α -grains of the RA Ti6Al4V and the crack path re-orientation in adjacent grains, thus highlighting the mechanisms behind the excellent CI resistance of this alloy.

ACKNOWLEDGEMENTS

The authors would like to gratefully acknowledge the financial support of the Swiss Federal Office for Defence Procurement (armasuisse).

REFERENCES

- [1] Suresh, S., Ritchie, R. O. (1984) Propagation of short fatigue cracks. *Inter Met Rev*, 29, 445-76.
- [2] Cottell G. (1954) Fatigue failures with special reference to fracture characteristics. *British engine technical report, vol. 2*, British Engine Boiler & Electrical Insurance Co., Ltd, Manchester, 221-256.
- [3] Barter S.A., Wanhill R.J.H. (2008). Marker loads for quantitative fractography of fatigue cracks in aerospace alloys. *National Aerospace Laboratory NLR*, Amsterdam.
- [4] Zapffe C.A. Clogg, Jr. M. (1945) Fractography—A New Tool for Metallurgical Research, *Trans. ASM*, 34, 71–107.
- [5] S.P. Lynch S.P., Moutsos S. (2006) A brief history of fractography. *J Fail Anal Prev*, 6, 54-69.
- [6] Abelkis, P. R. (1974): A Study of Fatigue Life and Crack Propagation under Flight-by-flight Loading Spectra, *IRAD Technical Report MDC-J5672*, Douglas Aircraft Company, Long beach, California.
- [7] Barter S., Dixon B. (2009) Investigation using quantitative fractography of an unexpected failure in an F/A-18 centre fuselage bulkhead in the FINAL teardown program. *Eng Fail Analy.* 16. 833–848.
- [8] Schijve, J. (1973): Effect of Load Sequences on Crack Propagation under Random and Program Loading, *Eng Frac Mech*, 5, 269-280.
- [9] AGARD-CP-376 (1984): Fatigue Crack Topography, Advisory Group for Aerospace Research and Development, Neuilly-sur-Seine.
- [10] Wanhill, R. J. H., Hattenberg, T. (2006): Fractography-based Estimation of Fatigue Crack “Initiation” and Growth Lives in Aircraft Components, NLR TP-2006-184, *NLR*, Amsterdam.
- [11] Lynch S.P. (2017). Some fractographic contributions to understanding fatigue crack growth. *Int. J Fatigue*, 104, 12-26
- [12] Barter, S., Burchill, M., Jones, M. (2017) Measured fatigue crack growth increments versus predictions for small cracks in 7XXX aluminium alloys. *Int J Fatigue* 105, 144–159.

- [13] Barter, S. A. (2003) Fatigue Crack Growth in 7050T7451 Aluminium Alloy Thick Section Plate with a Surface Condition Simulating Some Regions of F/A-18 Structure. DSTO-TR-1458, Department of Defence, Defence Science and Technology Organisation.
- [14] McDonald M, Boykett, R Jones M. (2012) Quantitative fractography markers for determining fatigue crack growth rates in aluminium and titanium aircraft structures, In Proc. of 28th Inter Conf of the Aeronautical Sc, ICAS2012, Brisbane, Australia.
- [15] Burchill, M., Barter, S., McDonald, M., Jones, M. (2015) The development of bar-coded marker band load sequences to enhance fatigue test outcomes. In Proc. of 16th Australian Aerospace Conf, 23-24 February 2015, Melbourne.
- [16] Sunder, R. (1983): Binary Coded Event Registration on Fatigue Fracture Surfaces, In Proc of the Inter Conf on Digital Techniques in Fatigue (SEECO '83), Ed., B.J. Dabell, Soc of Envi Eng, London, 197-218.
- [17] McDonald M. Boykett R. Jones M. (2013) Fatigue Testing of AA7050-T7451 with Various Corrosion Prevention Surface Treatments. DSTO-TR-2851, Department of Defence, Defence Science and Technology Organisation.
- [18] White, P., Barter, S. A., Molent, L. (2008): Observations of Crack Path Changes Caused by Periodic Underloads in AA7050-T7451, *Inter J of Fatigue*, 30, 1267-1278.
- [19] Krkoska M., White P., Barter S.A., Alderliesten R.C. Benedictus R (2010) Fatigue crack paths in AA2024-T3 alloy when loaded with constant amplitude and simple underloads spectra, *Eng Frac Mec*, 77, Issue 11, 1857-1865
- [20] Hall, J.A. (1997). Fatigue crack initiation in alpha beta titanium alloys. *Int. J. Fatigue*, 19, Supp. No. 1, S23-S37
- [21] Pilchak A. Williams, R. Williams, J. (2010) Crystallography of fatigue crack initiation and growth in fully lamellar Ti-6Al-4V. *Metal Mater Trans A* 41, 106-124
- [22] Stubbington C.A (1976) Metallurgical aspects of fatigue and fracture in titanium alloys. In Proc. AGARD 185, 3.1-3.19
- [23] Yuen, A., Hopkin, S.W., Leverant, G.R. Rau. C.A. (1974). Correlations between fracture surface appearance and fracture mechanics parameters for stage II fatigue crack propagation in Ti-6Al-4V. *Metal Trans B* 5, 1833-1842
- [24] Irving P.E. Beevers C.J. (1974) Microstructural influences on fatigue crack growth in Ti-6Al-4V, *Mat Sci & Eng.*, 14-3, 229-238.
- [25] Liu X. Sun C. Hong Y. (2016) Faceted crack initiation characteristics for high-cycle and very-high-cycle fatigue of a titanium alloy under different stress ratios, *Inter J Fatigue*. 92-2, 434-441.